Going fast with STM imaging

Leonard Gura, Zechao Yang, Heinz Junkes, Markus Heyde, and Hans-Joachim Freund, Fritz-Haber-Institut der Max-Planck-Gesellschaft, Berlin, Germany

Abstract

Scanning Tunneling Microscopy (STM) is a well established tool in surface science and is applied in related research fields. The large drawback of conventional raster STMs is the slow image acquisition of typically more than 100 s per image. This long acquisition time excludes the direct observation of dynamic processes occurring on sub-second timescales. Therefore, the development of high-speed STMs with the potential to acquire images in less than a second is promising for fundamental and applied research. In this article, the main approaches to increase the frame rate in STM are presented and discussed. The focus is on new unconventional spiral scan patterns.

Introduction

Scanning probe microscopy (SPM) provides information on surfaces and adsorbed species down to the atomic scale at different interfaces. Since the invention of scanning tunneling microscopy (STM) in the early 1980s,[1] numerous static sample systems have been investigated in ultra-high vacuum (UHV),[2–4] in a gas atmosphere,[5] and in liquid.[6–8] In liquid, the first atomically resolved STM images were reported in 1986.[9–12] Few years later, additional reference and counter electrodes were implemented to liquid STMs, which enabled true electrochemical in situ STM measurements.[13–15] A recent historic overview and an explanation of the fundamental working principles are provided in Ref. 16. The observation of structural formation as a function of time has been enabled by electrochemical STMs.[17] Recently, ultrahigh-resolution STM images were recorded in liquid and the molecular motion was registered without external stimulation.[18] This study is one example showing that the focus of STM investigations shifts from the investigation of static toward dynamic sample systems.

We must understand dynamic processes such as interactions at surfaces, thin film growth, and chemical reactions at the atomic scale to set the stage for future applications of the techniques in electrochemistry, biology, and materials science. Especially for electrochemical measurements at solid-liquid interfaces, the adsorption and desorption of surface species as well as the restructuring of surfaces under certain electrochemical conditions are of particular importance.[19] Directly related to these dynamic processes is the mobility of adsorbate species on surfaces, including atomic diffusion and migration mechanisms.

STM is a well established UHV surface science tool that is used to resolve surface structures, the atomic network of thin films, and the arrangement of adsorbed species due to its extraordinary spatial resolution. However, the time resolution of conventional STM is very low. Recording a single image often takes more than 100 s. Due to slow frame rates in conventional STMs, dynamics like diffusion processes, surface reactions, island growth, and the mobility of adsorbed molecules in general are not directly accessible.

The question arises how the outstanding spatial resolution of STM can be combined with improved time resolution. An increase in the frame rate leads to the possibility to directly observe individual dynamic processes. Due to the high number of acquired images, good statistics on these dynamic processes are possible. Most importantly, the shorter acquisition time and the possibility to investigate dynamic sample systems will lead to widespread applications in science and industry to study dynamics at the atomic scale.

To capture dynamics in UHV, the sample temperature can be adjusted ranging from cryogenic temperatures up to several 100 °C. In electrochemical STM, however the liquid limits the accessible temperature range considerably and the dynamics cannot be slowed down or speeded up as much as in UHV.[19] Therefore in liquid, the achievable frame rate determines—to an even greater extent than in UHV—which systems can be studied.

This limitation reinforces the importance to increase the imaging rate and therefore the achievable scan speed in STM.

The first attempt to record STM images at higher scan speeds was already undertaken in 1986—a few years after the invention of the STM.[20] The hexagonal graphite surface was imaged. Fig. 1A shows the original slow scan STM image of the graphite surface and Fig. 1B shows the filtered image.[21] The image was acquired with a line scan frequency of 10 Hz. The same group reported on fast scan STM images on graphite. They scanned with line scan frequencies of 1 kHz and averaged consecutive scans over time to generate the image shown in Fig. 1C. Fig. 1D shows the image with the superimposed ring structure. The hexagons show, that the acquired image is distorted. The distortion is attributed to the fast scan speed. The authors mention the advantages of high line scan frequencies, including the absence of low frequency noise, 1/f noise, and piezoelectric scanner hysteresis.[20]

Since then the advantages of high-speed scans were well known and efforts were made to increase the scan speed of STMs to capture physical phenomena that occur on much shorter timescales.[20,22–24] Still, it took more than 10 years before it was possible to capture dynamics at the atomic scale with the first video-rate STM acquiring up to 20 frames s^{-1}.[25] This long time for development provides an idea of the difficulties to successfully increase time resolution in STM without compromising its outstanding spatial resolution. The development of high-speed STMs involves various challenges, that are related to limitations of mechanical design, hardware, and software. The limitations and the approaches to overcome these limitations are discussed in the following sections of this article.

Video-rate STMs in both UHV and liquid have been developed now for more than 20 years.[25,26] The achievable frame rate increases and the perspective to scan with 1000 frames s^{-1} or more seems within reach. Still, only few groups scan beyond video-rate and so far only two groups operate electrochemical high-speed STMs.[26,27]

In contrast to high-speed STM, high-speed atomic force microscopy (AFM) as the alternative SPM technique is applied in many different research groups already. High-speed AFM provides sub-second resolution and is a versatile tool in electrochemistry,[28] biology,[29] and materials science.[30] AFM and STM share similar designs of the scanner unit. The factors that limit the scan speed in both SPM methods are almost identical, except for the different detection of the feedback signal. Therefore, the successful versatile use of high-speed AFM in many research fields, provides an idea of future applications of high-speed STM.

While conventional STM has found its way into industrial application, high-speed STM is only starting to getting commercialized. Add-on modules have been presented to enable fast STM.[31,32] With this development trend and the perspective to directly observe complex dynamic phenomena at the atomic scale, high-speed STM is promising for a broad field of applications. While STM continues to have tremendous impact in surface science, high-speed STM has great potential to extend its impact to the fast evolving fields of electrochemistry, biology, and materials science.[33]

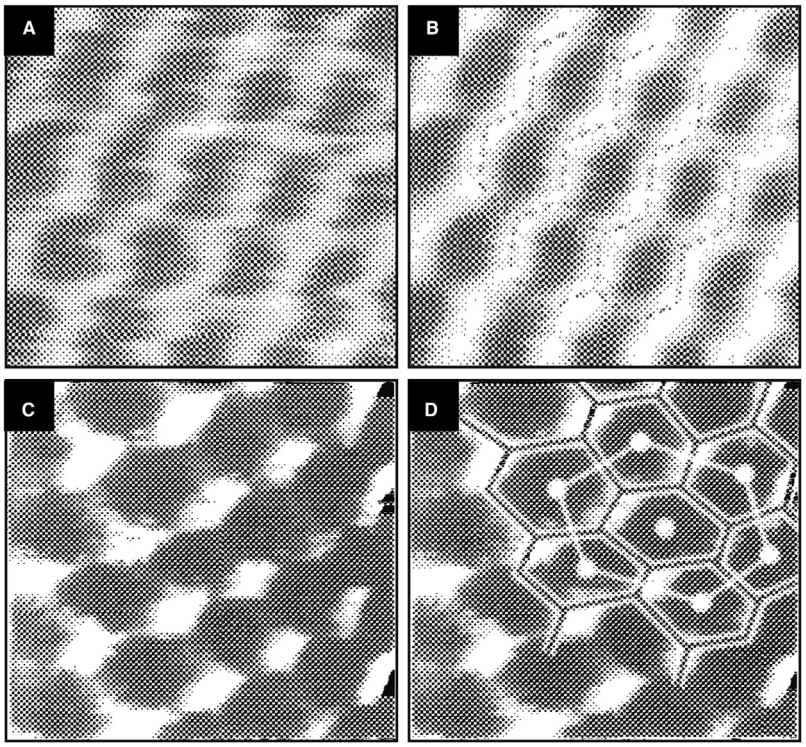

Fig. 1 (A,B) Slow scan STM images of graphite (10 mV, 5 nA, scan frequency 10 Hz). (C,D) Averaged fast scans STM images of HOPG (40 mV, 1 nA, scan frequency 1 kHz). (A,B) Reproduced from Ref. 21, with the permission of AIP Publishing; (C,D) Reproduced from Ref. 20, with the permission of AIP Publishing.

Limitations of high-speed STM

In general, STM designs must be mechanically stable to avoid interferences between scanner movement and mechanical resonances of the experimental setup. Therefore, the mechanical design asks for rigid and compact components that exhibit high resonance frequencies. This is especially true for STMs designed for high-speed scans. In literature, several designs are reported that lead to increased frame rates based on improved mechanical loops with high resonance frequencies.[19,24,34–44] Another approach is to analyze the mechanical properties of the STM to compensate for vibrations.[45] Besides the mechanical design, main limitations to increase the frame rate in conventional STM are (1) the slow electronic feedback that controls the tip-sample distance, (2) the slow data acquisition of hardware and software, (3) the conventional line-by-line raster scan geometry, which is inefficient and causes mechanical noise that distorts STM images considerably.

In the literature, several approaches exist to increase the frame rate in STM. Mechanical properties of the STM scanner, special preamplifiers, and slightly modified scan geometries have been explored.

Fig. 2 shows the schematic setup of the electronic hardware components of an STM. The real-time controller is accessed by an external computer that usually provides a graphical user interface (GUI) for the scan control. In this interface, scan parameters are set that shape the input signals for the STM scan. The signal is generated by the usage of one or more digital analog converters (DAC) and successively amplified. The amplified voltage input signal (V_I) is applied to the STM scanner, which results in lateral displacements of the STM tip. The tunneling current (I_T) between tip and sample surface is amplified by the preamplifier and digitized by the real-time controller. The measured tunneling current serves as input for the electronic feedback loop to control the tip-sample distance and is used to generate 2D images that are displayed on the external computer.

Every single component in this chain has physical limits determining its bandwidth. Table 1 summarizes exemplary bandwidths of the main state-of-the-art components that are commercially available.

As obvious from Table 1, the major limitation is the real-time control unit with its electronic feedback loop.

Electronic feedback

STM allows us to measure in constant current or in constant height mode. In conventional STM measurements, mostly the constant current mode is applied. In this mode, the electronic feedback of the real-time control unit of the STM adjusts the tip-sample distance to keep the tunneling current constant. Scanning at constant current provides, in addition to high lateral resolution, high vertical resolution. To increase the scan speed in constant current mode, the bandwidth of the electronic feedback control system must be high. Some approaches were made to acquire fast STM images in constant current mode.[24,35,36] However, the time constant of the feedback loop easily exceeds the mechanical resonance frequencies of the system. Therefore, mostly the constant height mode is used for high-speed STM.[25,31,32] In this mode, the tip-sample distance remains unchanged and the logarithm of the measured tunneling current is approximately proportional to the surface topography. Due to the non-linear dependence of current and tip-sample distance, the constant height mode is most suitable in measurements that focus on the lateral resolution on flat surfaces. To ensure good image contrast throughout the whole scan area, the tilting between the scanned plane and the sample surface must be considered. Especially at high scan speeds, the tilt correction is crucial to avoid tip crashes.

In addition to the constant current and the constant height modes, a so called hybrid mode is applied using the error signal of tip height in addition to the height signal.[39,50,51]

Depending on the STM design, other approaches to run the feedback loop are possible. Two independent feedback loops for fast and slow corrections were used e.g., in Refs. 24,35. Recently, the approach to use independent tube piezos was demonstrated,

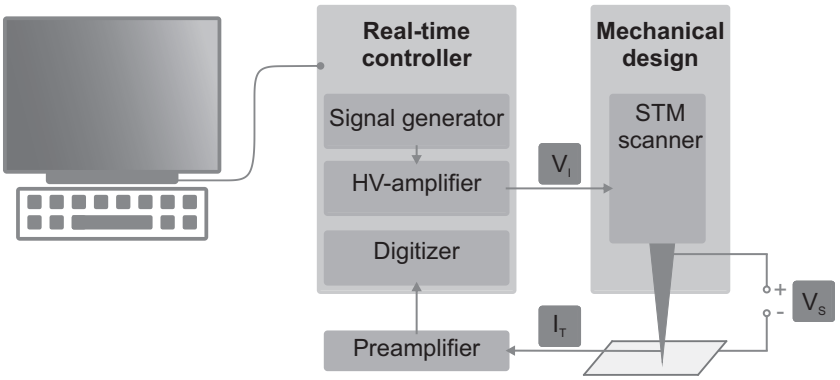

Fig. 2 Schematic of experimental setup of an STM. The electronic hardware components and their bandwidths are presented in Table 1. V_I is the input voltage for the STM scanner movement, I_T is the tunneling current, and V_S is the applied sample voltage. Adapted from Ref. 44, licensed under a Creative Commons Attribution (CC BY) license.

Table 1 Bandwidths of commercially available hardware components for high-speed applications in comparison to the electron tunneling limit.

Electronics	*Bandwidth (Hz)*	*Time constant (s)*	*Refs.*
Electron tunneling	3 G (1 nA)	0.33 n	41
Real-time controller	30 k	33 μ	46
Preamplifier	600 k (10^9 *V/A*)	1.7 μ	47
Digitizer	250 M	4 n	48
HV amplifier	5 M	200 n	49

Table taken from Ref. 44, licensed under a Creative Commons Attribution (CC BY) license.

assigned to slow conventional scans and high-speed scans, respectively.[44] When the small tube piezo scans at high speeds, the slow feedback loop runs on the larger tube piezo that is used for conventional scans.

For all modes mentioned above, the preamplifier must provide output signals with a good signal to noise ratio. As listed in **Table 1**, the preamplifier bandwidth is the second lowest one. Therefore, choosing preamplifiers with high bandwidth is crucial to obtain high resolution images at high speed. Shortening the wire loop by locating the preamplifier close to the scan head further improves the signal-to-noise ratio.[39] Various approaches are presented in the literature that use special preamplifier designs.[31,32,35,39,52–54] A detailed discussion on the preamplifier noise and the stability of preamplifiers in the context of high-speed STM measurements is provided in Ref. 51. In this article, we focus on possibilities to increase the scan speed with commercial state-of-the art preamplifiers, as listed in **Table 1**, for instance.

When scanning above the cut-off frequency of the preamplifier, strong oversampling is necessary.[32] The oversampling is directly related to the data acquisition, which is addressed in the following section.

The improvement of the limiting electronic components that are part of the electronic feedback loop mentioned above, will not only increase the achievable frame rate for high-speed STM, but will also improve the image contrast in conventional STM measurements.

Data acquisition

At high frame rates, high data sampling frequencies are required. As mentioned above, this is especially true when strong oversampling is required due to scanning above the cut-off frequency of the preamplifier. Up to now, most conventional STM hardware is not designed for high-speed data acquisition. However, some conventional STM controllers provide additional digital input channels with data sampling rates up to 200 MHz.[46] With openly accessible protocols they can, in principle, be used to acquire high-speed STM scans.

Another approach is to use custom programmed hardware to generate the input signals and to acquire the data.[19,31,32,55] The add-on instrument that can be combined with commercial STMs to scan at high-speed is the first step toward broader applications of high-speed STMs.[31,32] Another convenient solution is to combine commercial and custom-designed scan hardware by using independent piezo-actuators as slow and fast scanners, respectively.[44,55] Here, fast digitizing units can be used with sampling rates of 250 MHz and beyond.

Apart from the analog to digital converter to acquire the data from the preamplifier, the real-time processing speed and data transfer must be considered at high scan rates. As discussed in Ref. 31, an image of 200 × 200 pixels with 16 bit resolution and acquired with a rate of 100 Hz needs at least 64 Mbit s^{-1} data stream. In this calculation the oversampling of data is not considered.

The continuous improvement of electronics and computer power facilitates the collection of larger data sets. For the challenge of collecting, processing, and storing large amounts of data, interdisciplinary approaches are promising.

To avoid data loss, special designs have been realized. Separate memories were implemented collecting and transferring the data in an alternating manner.[31] Different groups separated the image display and the data acquisition threads.[19,56] The data acquisition is realized in different buffers. Magnussen et al. use a ring buffer that can buffer the last minutes of the measurement and is saved upon users request.[19] We implemented a queue of adjustable size that buffers the data before it is stored to one or several hard drives.[56] In principle, infinite scan series are possible, because the data can be accessed from several local computers and the acquired data are assigned in real-time by timestamps.[56] This design enables to run completely independent live monitors of the high-speed STM images. To save the data different formats are possible. The Hierarchical Data Format version 5 (HDF5) is favorable due to its adjustable data structure and functions like single writer multiple reader (SWMR).[32,56]

For the new dataformats, data visualization and analysis tools are developed.[32,56] Our freely accessible, purely python based software can handle conventional images as well as data that contains spatial coordinates and intensity values.[56,57] The latter function enables the visualization, the processing, and the analysis of data that does not match the regular grid of conventional 2D images. Various methods exist to reconstruct 2D grid images from the non-raster STM data point cloud.[32,56] Examples of such unconventional scan data is presented in the following sections.

Scan geometry

Conventional raster scan

Conventionally, STM images are acquired with line-by-line scans as shown in Fig. 3. The triangles in Fig. 3A and B represent data acquisition points. One and only one acquisition point is within one grid point of the overlaid 2D grid. This perfect match enables the representation as 2D images without additional calculations. In the last century, calculations for image reconstructions were limited considerably by available computational power. Due to the convenient mapping of raster data points to the 2D image grid, the raster scan geometry was chosen and the same geometry is generally applied in SPM to date. However, in STM and other SPM techniques the line-by-line motion has considerable drawbacks. One drawback is that the data is not acquired continuously. After each line, the tip must travel back. This backward motion of the tip multiplies the acquisition time per image. Furthermore, during this rapid change of the propagation direction and the velocity of the tip, the image contrast can change considerably.

The larger drawback is the scan motion itself and the input that is applied to the STM scanner. The sharp points of inversion in the triangular piezo input signal, shown in Fig. 3C, result in rapid changes of the tip propagation direction. This in turn introduces mechanical resonances into the system and distorts the STM images. These distortions become severe at increased scan speeds.

In the literature several approaches are discussed to avoid mechanical resonances by changing the scan geometry in SPM.[58–68] While in AFM, unconventional scan geometries were tested and applied within experimental setups,[60–62,66,68–72] STM sticks to the raster paradigm. Recently, the first unconventional scan patterns were applied to increase the frame rate in STM.[44,56,73,74] Examples of STM images acquired with unconventional scan geometries are shown in the following sections of this article.

For the scan geometry, the general aim is to smooth the scan input signals for the lateral displacement of the STM tip. At the same time, the real space must be scanned efficiently. Considering these constraints, sinusoidal raster, Lissajous and spiral geometries are compared.[66] Fig. 4 provides an overview of these geometries and their input signals.

Teo et al.[66] consider these different scan geometries and evaluate their advantages and disadvantaged for SPM with focus on AFM applications. Therefore, the length scales in Fig. 4 are on the micrometer scale. For STM, the nanometer scale would be more adequate. For SPM techniques that require a vertical feedback system, they conclude that the sinusoidal raster scan is most favorable in terms of sampling frequency, probe velocity, and topography bandwidth. The following section reports examples of sinusoidal raster scans applied to STM.

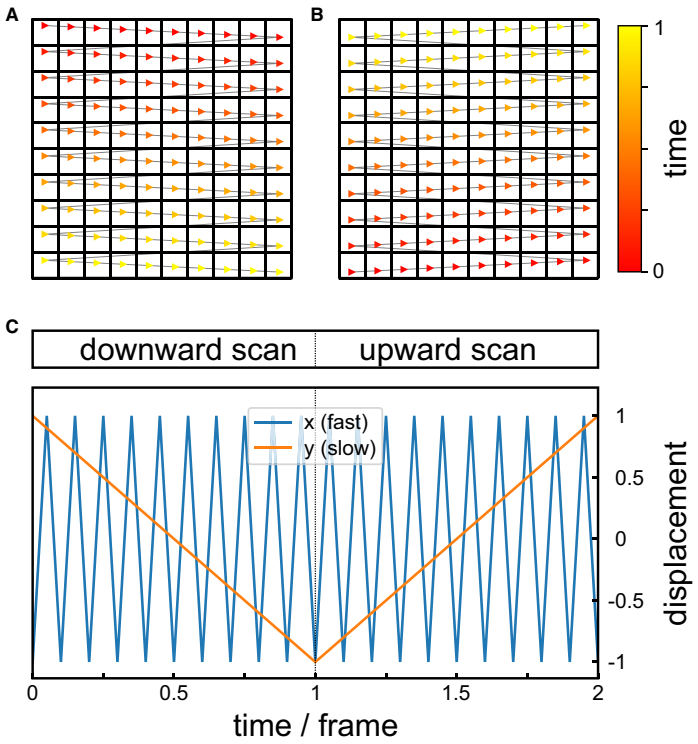

Fig. 3 Schematic of the raster scan in conventional STM. (A) Downward raster scan. (B) Upward raster scan. For visualization, only the forward scans are displayed. The small red and yellow triangles represent data acquisition points and indicate the tip propagation direction. The gray lines represents the tip trajectory. The 2D grid is overlaid. Each grid point contains one data acquisition point. (C) Corresponding signal of the piezo displacement as a function of time. Adapted from Ref. 56, licensed under a Creative Commons Attribution (CC BY) license.

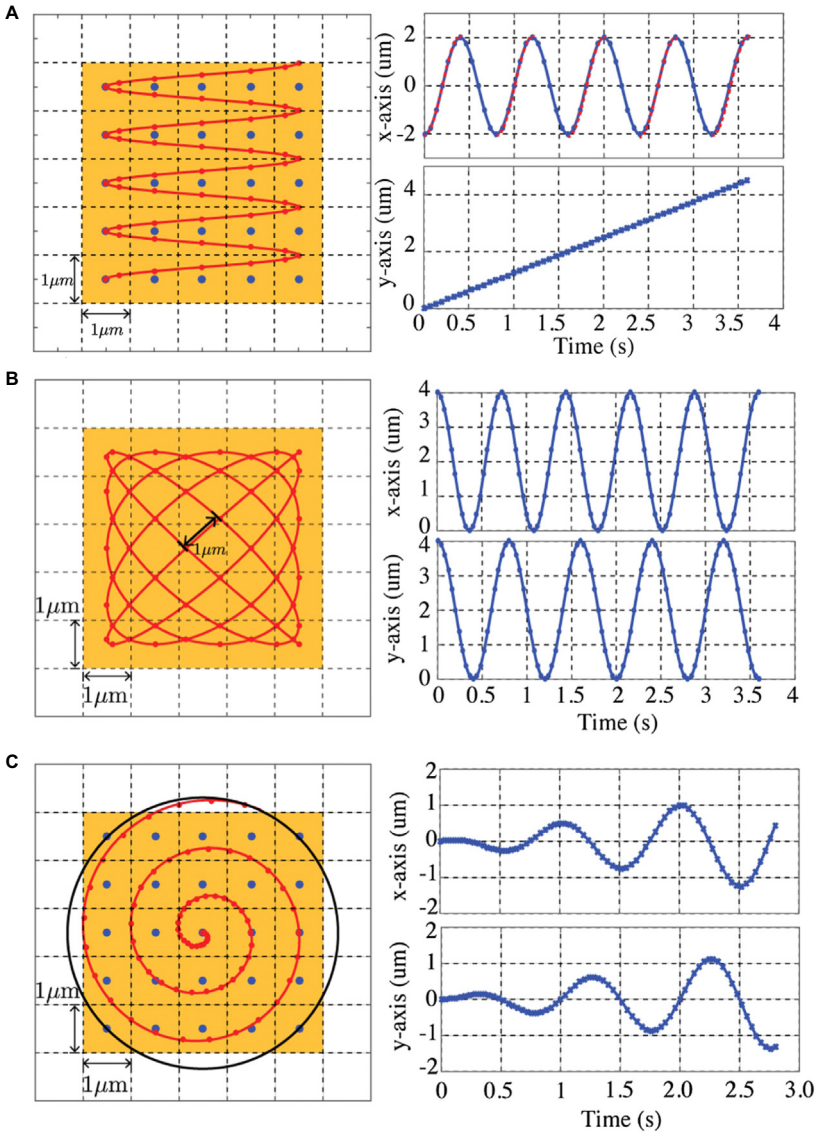

Fig. 4 Comparison of different high-speed SPM scan patterns. (A) Sinusoidal scan. (B) Lissajous scan. (C) Spiral scan. Corresponding signal of the piezo displacement in *x*- and *y*-direction as a function of time. Adapted from Ref. 66 with permission. Copyright by 2016 Chinese Automatic Control Society and John Wiley & Sons Australia, Ltd.

Sinusoidal raster scan

The first high-speed STM measurements that resolved dynamics at the atomic scale used the sinusoidal raster scan pattern, which uses a sine wave in the fast scan direction.[25] The advantages of the sinusoidal raster scan is that the scan pattern is very similar to the conventional raster scan and therefore makes its implementation much easier. In principle, the sinusoidal raster scan does not necessarily require custom hardware and software. These might be the reasons why, nowadays, the most common modification of the scan geometry is the sinusoidal raster scan.[31,32,36,39,41,43,54] Although additional calculations for image reconstruction and distortion corrections are needed,[32,39,40,75,76] the sinusoidal raster scan was the only alternative in high-speed STM until recently. Fig. 5 shows an exemplary collection of high-speed sinusoidal raster images from literature. The examples range from the first published results[25] to most recent publications and include measurements in UHV, ambient, and liquid.

Fig. 5A shows the first atom dynamics captured with high-speed STM.[25] Oxygen diffusion on Ru(0001) could be monitored and analyzed in real space and in real time. In the following section, the same sample system will be resolved by spiral high-speed STM. Related sample systems are of great interest to date. Fig. 5B shows the oxygen diffusion on CO/Ru(0001), which revealed a door-opening mechanism for diffusion.[77] Both systems in Fig. 5A and B were acquired at similar frame rates of 6 and 10 Hz, respectively. Fig. 5C–F shows the graphite (HOPG) surface. The image contrast at higher scan rates improved considerably compared to the example in Fig. 1. However, the images are not free of distortions. Especially at the edges of the images distortions are present.

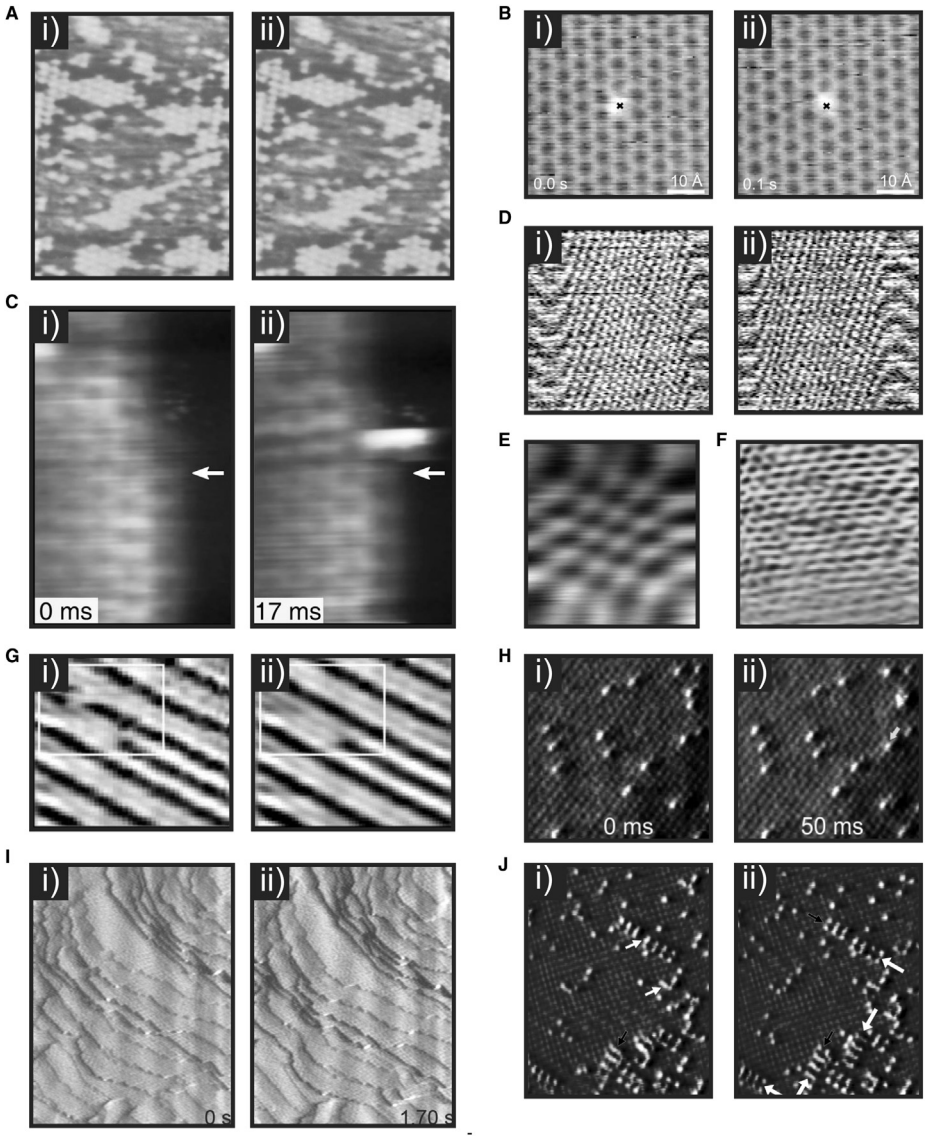

Fig. 5 Collection of sine wave high-speed STM images. (A) Adsorbed oxygen on Ru(0001) ($V_S = -1.6$ V, $I_T = 3$ nA, scan area $= 8 \times 19$ nm^2, T = 300 K 6 frames s^{-1}). (B) O atom embedded in CO/Ru(0001) ($V_S = -0.22$ V, $I_T = 10$ nA, scan area $= 5 \times 5$ nm^2, T = 300 K, 10 frames s^{-1}). (C) Klein (k) edges of a top-fcc EG layer on Ni (111) ($V_S = 0.02$ V, $I_T = 7$ nA, scan area $= 1.6 \times 2.5$ nm^2, T = 710 K, 60 frames s^{-1}). (D) HOPG ($V_S = -0.1$ V, $I_T = 1$ nA, 80 frames s^{-1}). Trace (left to right) and retrace (right to left) are shown. (E) HOPG (T = 300 K, 52 frames s^{-1}). (F) Graphite (T = 300 K, 40 frames s^{-1}). (G) Deconstruction of the Rh(110)-c(2 × 8) oxygen structure in hydrogen atmosphere (T = 473 K, 100 frames s^{-1}). (H) S_{ad} diffusion on c(2 × 2)-Cl_{ad}-covered Cu(100) in 0.01 M HCl at −0.32 V versus a standard calomel electrode (20 frames s^{-1}). (I) Electrodeposition of Cu from a 10 mM $CuSO_4$ and 0.1 M H_2SO_4 solution at −40 mV versus Cu/Cu^{2+} ($V_S = 5$ mV, $I_T = 500$ pA, scan area $= 155 \times 200$ nm^2, 1.2 frames s^{-1}). (J) CH_3S_{ad} on Cu(100) in 0.01 M HCL at −0.32 V versus a standard calomel electrode (scan area $= 12.2 \times 15.2$ nm^2, 10 frames s^{-1}). Images labeled with i) and ii) show consecutive images of the same scan sequence. (A) Reprinted from Ref. 25, Copyright 1997, with permission from Elsevier Science B.V; (B) From Ref. 77. Reprinted with permission from AAAS; (C) From Ref. 78. Reprinted with permission from AAAS; (D) Reproduced from Ref. 39, with the permission of AIP Publishing; (E) Reproduced from Ref. 75, with the permission of AIP Publishing; (F) Reprinted from Ref. 32, Copyright 2019, with permission from Elsevier B.V; (G) Reproduced from Ref. 31, with the permission of AIP Publishing; (H) Adapted from Ref. 19 with permission. Copyright 2019 Wiley-VCH Verlag GmbH & Co. KGaA, Weinheim. Copyright by 2019 Wiley-VCH Verlag GmbH & Co. KGaA, Weinheim; (I) Reproduced from Ref. 27, with the permission from AIP publishing; (J) Adapted with permission from Ref. 79. Copyright 2012 American Chemical Society.

Fig. 5G shows the dynamics of missing rows on the Rhodium surface[31] and Fig. 5H provides an example of high-speed STM measurements in liquid that reveals surface diffusion of adsorbed sulfur. Fig. 5I shows large electrochemical STM images exceeding length scales of 100 nm that reveal the electrodeposition of Copper. Every image is acquired within 0.85 s while flowing the electrolyte. In Fig. 5J, the short CH_3S_{ad} stripes are identified as the internal structure of the formed clusters by STM measurements in liquid.

STM measurements in liquid involve challenges including the influence of the tip-sample capacitance, the lower tunneling barrier heights compared to vacuum, and the viscosity of the liquid phase. Especially the latter one affects high-speed measurements and is related to interfering lower resonance frequencies of the scanning probe immersed in the liquid phase. Similar effects have been observed for AFM cantilevers in liquids, as for instance described in Ref. 41. Comprehensive overviews and discussions of high-speed STM in liquid electrolytes are provided in Refs. 19,51.

Table 2 lists different image rates that have been achieved so far including most of the studies shown in Fig. 5.

Spiral scan

As mentioned above, Teo et al.[66] concluded that the sinusoidal raster is favorable for systems that require a vertical feedback loop and until recently high-speed STM solely used this sinusoidal raster pattern as variation from the conventional raster scan pattern.

However, as mentioned in the Electronic feedback section, STM can operate in constant height mode with no or only very slow feedback loop parameters. Without this limiting feedback loop, other scan geometries might be favorable that can shift from the inefficient raster scans toward unconventional scan geometries.

In contrast to STM, in other scanning microscopy techniques, the paradigm to use the raster geometry seems to be broken already.[62,63,65,80,81]

Comparing the most promising scan geometries in Fig. 4, it becomes obvious that the spiral scan in Fig. 4C takes less time to scan the real space. Furthermore, the sine and cosine input signals of the spiral scan exhibit lower frequencies compared to the sinusoidal raster scan in Fig. 4A and the Lissajous scan in Fig. 4B. The waveform of the spiral limits the triggering of resonance frequencies. The data acquisition points of the spiral geometry do not coincide with the 2D grid. However, the point density in the center of the spiral is increased, while for the Lissajous scan, the point density at the edges increases.

Considering the scan without accounting for the data representation, the spiral geometry is favored. In fact, the spiral geometry was already applied 10 years ago to correct image distortions in slow scan images.[59,82] In principle, spiral trajectories can also improve slow scan STM images due to reduced excited resonance frequencies.

Fig. 6 shows the schematic spiral trajectory as a function of time. The spiral scan input signals consist of smooth sine and cosine waves for both lateral scan directions. Outward and inward scans are shown that are smoothly connected to avoid rapid changes of the tip velocity and the propagation direction.

The spirals in Fig. 6 show constant angular velocity scans. The spiral trajectory can be modified based on the measurement requirements. Parameters a and b in Eqs. (1) and (2), for instance, can tune the spiral geometry and the tip velocity along its trajectory.

$$x = t^a \cdot \cos\left(\omega \cdot t^b\right) \tag{1}$$

$$y = t^a \cdot \sin\left(\omega \cdot t^b\right) \tag{2}$$

x and y are the spatial coordinates. They directly relate to the voltage input signal for the scanner and are drawn in Fig. 6C. t is the time and ω is the frequency that resembles the number of rotations per frame. Thus, ω adjusts the line density of the spiral scan for a given geometry, which is also referred to as the pitch size. The shown spiral in Fig. 6 is generated by setting parameters $a = b = 1$. This results in an Archimedean spiral with constant angular velocity (CAV). As mentioned above, the tilt correction is crucial for constant height or quasi constant height measurements. This is true for sinusoidal scans[31] and for spiral scans.[56] The tilt correction can easily be added to the input signal for any STM design.

In recent publications, the first application of spiral scan patterns to increase the scan speed and the frame rate was presented.[44,56,73,74] The spiral scans were performed on the oxygen covered Ru(0001) surface. This is the sample system that was investigated by the first break-through experiment of high-speed STM measurements 25 years ago by Wintterlin et al.[25] O/Ru(0001) and related sample systems are relevant for catalysis and thin film growth.[77,83–88]

Table 2 Frame rates of state-of-the-art high-speed STMs and the corresponding scanning parameters.

Environment	*Sample system*	*Image size (nm²)*	*Resolution*	*Frame rate (Hz)*	*Refs.*
RT-UHV	O Diffusion on Ru(0001)	8 × *8*	Atomic	15	25
Liquid	S Diffusion on Cu(100)	9.4 × *9.4*	Atomic	20	19
Ambient	HOPG	1 × *1*	Atomic	52	75
LT-UHV	Molecular self-assembly	6 × *6*	Submolecular	60	32
HT-UHV	Graphene growth on Ni(111)	1.5 × *3*	Atomic	60	78
RT-UHV	HOPG	5 × *5*	Atomic	80	39
HT-UHV	Surface reconstruction of Rh(110)	6.5 × *6.5*	Atomic row	100	31
RT-UHV	O Diffusion on Ru(0001)	5 × *5*	Atomic	120	56

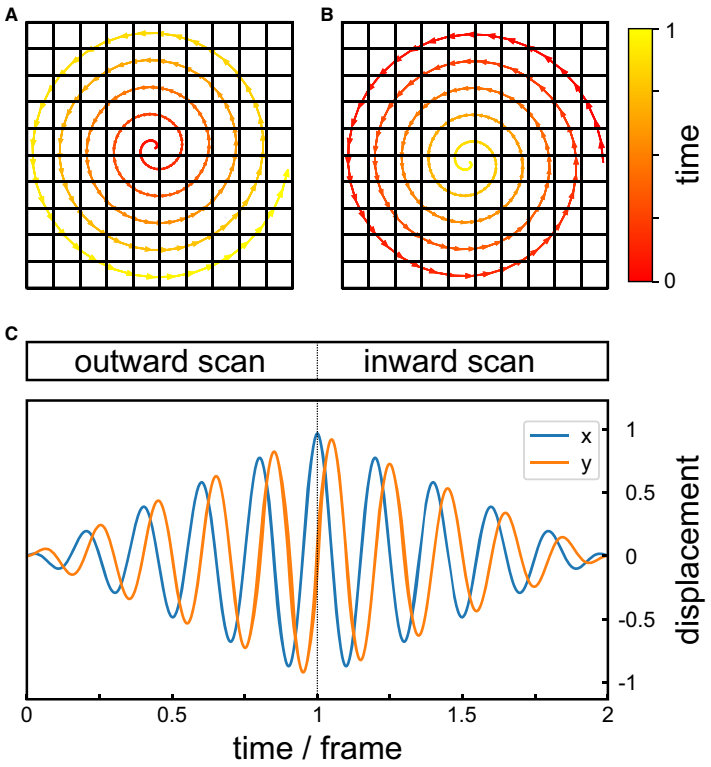

Fig. 6 Schematic of the spiral scan geometry. (A) Outward spiral scan. (B) Inward spiral scan. The small red and yellow triangles represent data acquisition points and indicate the tip propagation direction. The gray lines represents the tip trajectory. The 2D grid is overlaid. Each grid point contains one data acquisition point. (C) Corresponding signal of the piezo displacement as a function of time. Adapted from Ref. 56, licensed under a Creative Commons Attribution (CC BY) license.

Fig. 7 shows atomically resolved high-speed spiral images at different frame rates. The upper row shows the raw data only visualized by a 2D histogram. This is the image contrast of the live monitor mentioned above. Individual atoms can be identified. The data were not filtered, no drift, and no distortion correction was done. It appears that in contrast to sinusoidal raster scans that require artifact corrections,[19] the spiral scan does not require artifact nor distortion corrections. For comparison, the filtered data are shown in the lower row of Fig. 7.

So far consecutive images could be acquired in 8.3 ms, which corresponds to frame rates of 120 Hz. The scan speed in these spiral scans with frame rates of 120 Hz exceeds 200.000 nm s^{-1}, which is beyond scan speeds of sinusoidal scans in e.g., Refs. 19,31,39. The fact that the STM can scan in spiral motion with such high scan speeds affirms that this trajectory is favorable. It is worth noting that the limits in acquiring consecutive images at more elevated frame rates was so far not the scan motion itself.

Fig. 8 gives an idea about the dynamics of the adsorbed oxygen atoms on the Ru(0001) surface. Dynamics can be captured within 8.3 ms. However, not in every consecutive frame dynamic processes are detected. For instance, the configuration in Fig. 8A and B is similar. In various measurements at frame rates of 20, 30, 40, and 120 Hz, the same oxygen mobility was detected. This indicates that frame rates in the order of 20 Hz are sufficient to access the dynamics of this sample system at room temperature. As pointed out by Magnussen,[19] the frame rate should be in the same order of magnitude as the dynamic processes.

Similar as for the individual oxygen species, the dynamics in the O (2×2) adlayer on Ru(0001) were in the same range in measurements with frame rates of 20 and 40 Hz.[73] In this study, another advantage of spiral scans becomes obvious. As mentioned above, the CAV spiral exhibits high data point density in the center. In addition, due to the continuous scan in inward and outward direction, the center of the spiral is resolved in shorter timespans than the overall frame rate. In the shown case in Fig. 9, the center of the spiral was acquired within 16 ms while the whole scan took 50 ms. This enabled the resolution of the occupied intermediate state along the oxygen diffusion pathway in the O (2×2)/Ru(0001) layer.[73]

In contrast to our finding of an intermediate diffusion state of O on Ru, Besenbacher noted in the year 2005 that monitoring the transition of diffusing species will remain out of reach for high-speed STM.[33] However, in the present study we could show that with adequate sample systems that include metastable states along the diffusion pathway, high-speed STM can go beyond the observation of discrete hopping events.

For higher oxygen overages, dynamic formations of O (2×1) islands on Ru(0001) were observed. Fig. 10 shows the high-speed spiral images that resolved fast flipping events of O (2×1) 1D lines and long term reorientation of differently oriented O (2×1)

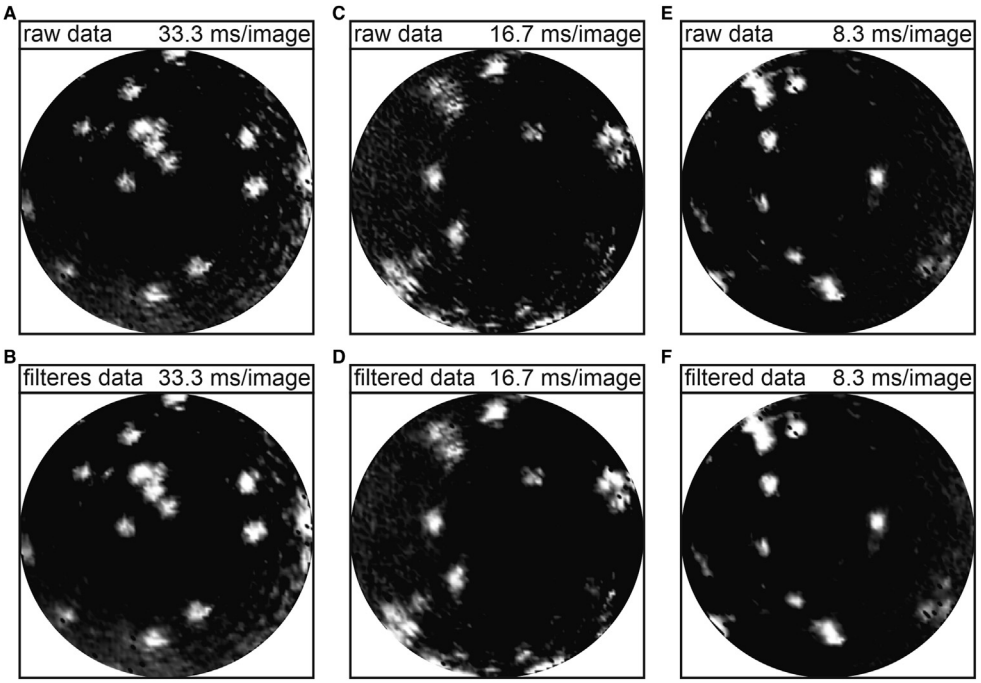

Fig. 7 Atomically resolved spiral STM images. The images show the Ru(0001) surface with a low oxygen coverage in UHV at 300 K. The acquisition time per image is displayed at the top right of each image and ranges from 33.3 ms down to 8.3 ms. (A,C,E) Unfiltered raw data visualized by 2D histograms. (B,D,F) 2D histogram with applied 2D Gaussian filter (scan diameter = 5.0 nm, a slow feedback for keeping an average $I_T = 2.0$ nA, $V_S = 0.9$ V). Adapted from Ref. 44, licensed under a Creative Commons Attribution (CC BY) license.

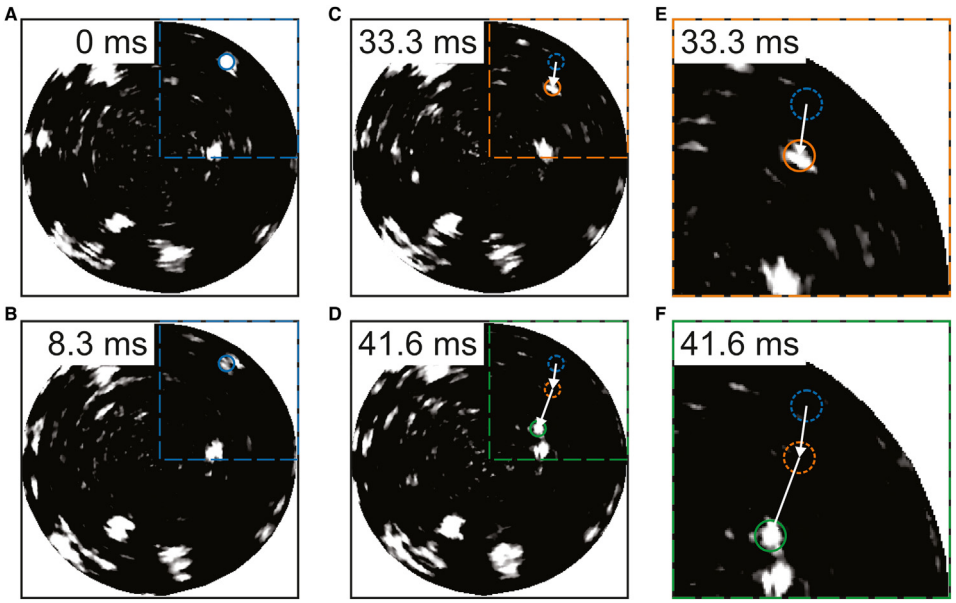

Fig. 8 Dynamics at the millisecond timescale on the oxygen covered Ru(0001) surface. The images relate to **Fig. 7**. Moving oxygen species are color coded and their trajectories are marked with white arrows (scan diameter = 5.0 nm, a slow feedback for keeping an average $I_T = 2.0$ nA, $V_S = 0.9$ V). Adapted from Ref. 56, licensed under a Creative Commons Attribution (CC BY) license.

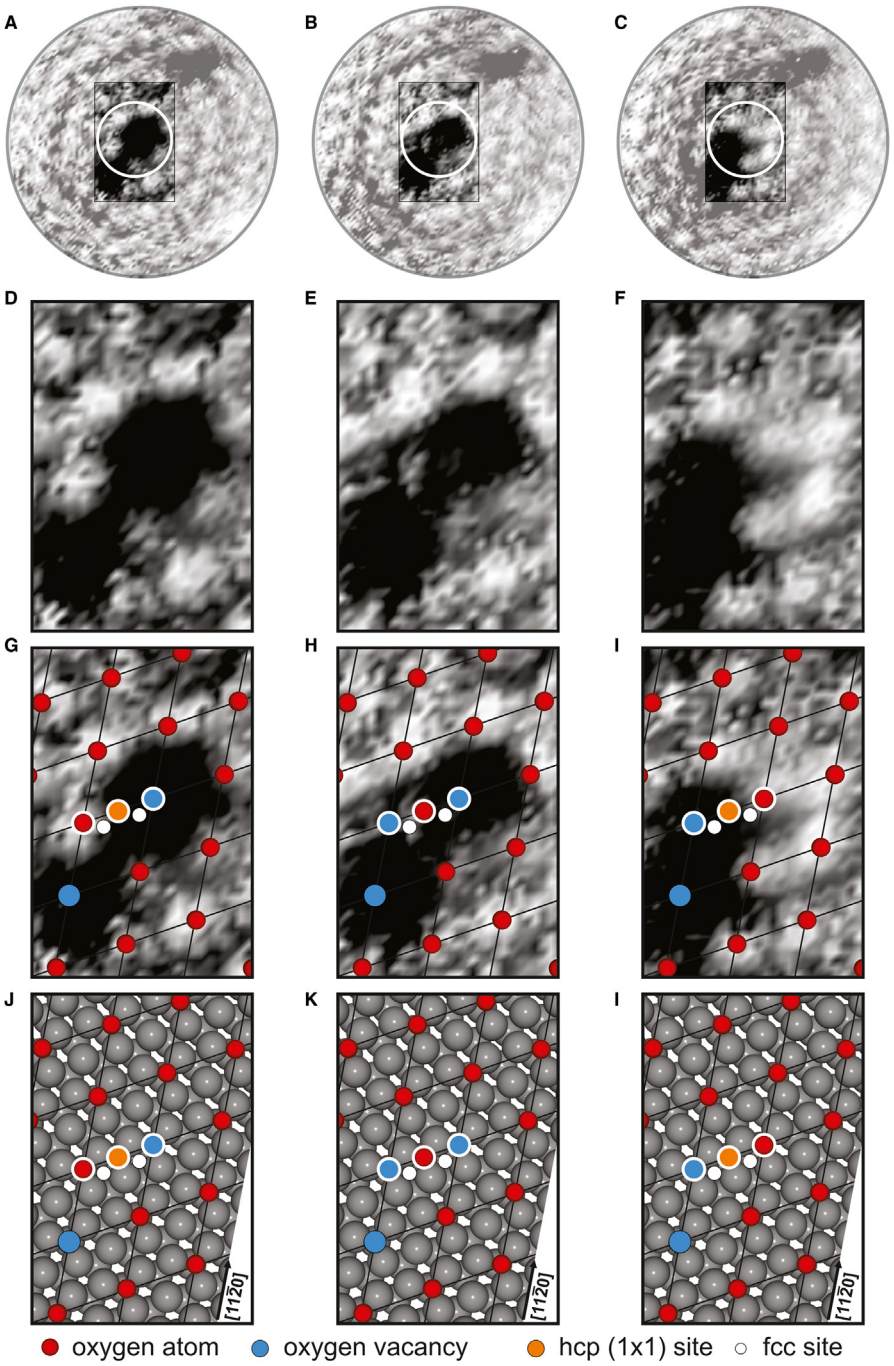

Fig. 9 Resolved intermediate state of the oxygen diffusion. Atomically resolved spiral STM images of the O(2 × 2)/Ru(0001) surface in UHV at 300 K. (A–C) Three consecutive spiral STM images (i.e., inward, outward, inward scans) (acquisition time = 50 ms, scan diameter = 5.0 nm, a slow feedback for keeping an average $I_T = 1.4$ nA, $V_S = 1.0$ V). The region of interest in the white circle is acquired within 16 ms. (D–F) show the magnified scan regions highlighted in (A–C), respectively. (G–L) show the corresponding structural model. Taken from Ref. 73.

domains. As mentioned above, scan series can be recorded over very long timespans. This enabled the investigation of elementary dynamics at the atomic scale that lead to mesoscopic changes on longer timescales.

We successfully applied spiral scans to acquire high-speed STM images in UHV and in ambient conditions. Due to the adjustable geometry and the tunable tip speed spirals scans are promising to resolve several sample systems, including solid-liquid interfaces. In combination with improved electronic components, and fast data acquisition, dynamic processes occurring on short timescales of milliseconds can be accessed. Not only faster processes become accessible due to further improved STM frame rates, but also the fast dynamics can be related to larger timescale phenomena that might range over several seconds, minutes or even hours.

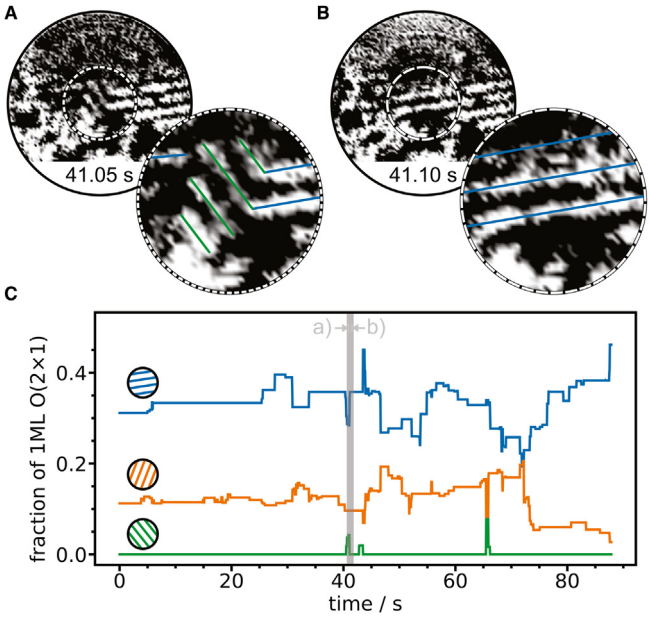

Fig. 10 Fast structural changes in the O(2 × 1) adlayer on Ru(0001). (A,B) Spiral STM images acquired in 50 ms in UHV at 300 K (scan diameter = 9.0 nm, a slow feedback for keeping an average $I_T = 1.0$ nA, $V_S = 1.0$ V). The 1D line orientations are highlighted with color coded straight lines the insets at the bottom right. (C) plots the evolution of the normalized length of these 1D lines with different orientations. Reproduced from Ref. 74 with permission from the Royal Society of Chemistry.

Concluding remark

Reviewing the literature from the last decades, it becomes obvious that many parameters play a crucial role when the scan speed of STM should be increased. Paradigm shifts as the usage of unconventional scan patterns are promising to set the stage for new speed records. These new achievements can reveal high complexity in supposedly simple and well understood sample systems.[19,56,73]

High-speed STM is an evolving field with the great potential to elucidate dynamics at the atomic scale in real space and real time. Particle-particle-, particle-substrate- interactions, dissolution and growth processes of thin films become accessible. Resolving these dynamics on shorter timescales leads to better understanding of critical processes in physical, chemical, and especially in catalytic reactions.[89] The study of these fundamental processes prepare the ground for future applications in electrochemistry, biology, and materials science.

Acknowledgments

We acknowledge the software development of Matthias Brinker, Patrik Marschalik, and William Kirstaedter that enabled the operation of the high-speed STM. We thank Florian Kalaß for working on the graphical user interface of the scan control and the data analysis. We thank Jens Hartmann for his design concepts for the mechanical components of our UHV-STM. Furthermore, we thank the mechanical workshop and the electronics workshop of the FHI for support and manufacturing. We thank Wolf-Dieter Schneider for fruitful discussions throughout the last years. This project has been financed by the European Research Council (ERC) under the European Union's Horizon 2020 research and innovation program (grant agreement CRYVISIL–REP-669179). LG acknowledges support by the IMPRS EPPC.

References

1. Binnig, G.; Rohrer, H.; Gerber, C.; Weibel, E. Surface Studies by Scanning Tunneling Microscopy. *Phys. Rev. Lett.* **1982,** *49,* 57–61. https://doi.org/10.1103/PhysRevLett.49.57.
2. Binnig, G.; Rohrer, H.; Gerber, C.; Weibel, E. 7 ×7 Reconstruction on Si(111) Resolved in Real Space. *Phys. Rev. Lett.* **1983,** *50,* 120–123. https://doi.org/10.1103/PhysRevLett.50.120.
3. van Hove, M.; Cerda, J.; Sautet, P.; Bocquet, M.-L.; Salmeron, M. Surface Structure Determination by STM vs LEED. *Prog. Surf. Sci.* **1997,** *54* (3), 315–329. https://www.sciencedirect.com/science/article/pii/S0079681697000117.
4. Kresse, G.; Schmid, M.; Napetschnig, E.; Shishkin, M.; Köhler, L.; Varga, P. Structure of the Ultrathin Aluminum Oxide Film on Nial(110). *Science* **2005,** *308* (5727), 1440–1442. https://doi.org/10.1126/science.1107783.
5. Magonov, S. N. Surface Characterization of Materials at Ambient Conditions by Scanning Tunneling Microscopy (STM) and Atomic Force Microscopy (AFM). *Appl. Spectrosc. Rev.* **1993,** *28* (1–2), 1–121. https://doi.org/10.1080/05704929308021499.
6. Itaya, K. In Situ Scanning Tunneling Microscopy in Electrolyte Solutions. *Prog. Surf. Sci.* **1998,** *58* (3), 121–247. https://doi.org/10.1016/S0079-6816(98)00022-7.

7. Gewirth, A. A.; Niece, B. K. Electrochemical Applications of In Situ Scanning Probe Microscopy. *Chem. Rev.* **1997,** *97* (4), 1129–1162. https://doi.org/10.1021/cr960067y.
8. Hommrich, J.; Hümann, S.; Wandelt, K. Cadmium Underpotential Deposition on Cu(111) In Situ Scanning Tunneling Microscopy. *Faraday Discuss.* **2002,** *121,* 129–138. https://doi.org/10.1039/B200406M.
9. Drake, B.; Sonnenfeld, R.; Schneir, J.; Hansma, P. K.; Slough, G.; Coleman, R. V. Tunneling Microscope for Operation in Air or Fluids. *Rev. Sci. Instrum.* **1986,** *57* (3), 441–445. https://doi.org/10.1063/1.1139208.
10. Sonnenfeld, R.; Schardt, B. C. Tunneling Microscopy in an Electrochemical Cell: Images of Ag Plating. *Appl. Phys. Lett.* **1986,** *49* (18), 1172–1174. https://doi.org/10.1063/1.97405.
11. Sonnenfeld, R.; Hansma, P. K. Atomic-Resolution Microscopy in Water. *Science* **1986,** *232* (4747), 211–213. https://www.science.org/doi/pdf/10.1126/science.232.4747.211.
12. Schneir, J.; Hansma, P. Scanning Tunneling Microscopy and Lithography of Solid Surfaces Covered With Nonpolar Liquids. *Langmuir* **1987,** *3* (6), 1025–1027.
13. Lustenberger, P.; Rohrer, H.; Christoph, R.; Siegenthaler, H. Scanning Tunneling Microscopy at Potential Controlled Electrode Surfaces in Electrolytic Environment. *J. Electroanal. Chem. Interfacial Electrochem.* **1988,** *243* (1), 225–235. https://doi.org/10.1016/0022-0728(88)85043-5.
14. Itaya, K.; Tomita, E. Scanning Tunneling Microscope for Electrochemistry—A New Concept for the In Situ Scanning Tunneling Microscope in Electrolyte Solutions. *Surf. Sci.* **1988,** *201* (3), L507–L512. https://doi.org/10.1016/0039-6028(88)90489-X.
15. Allongue, P.; Costa-Kieling, V.; Gerischer, H. Etching of Silicon in NaOH Solutions: I. In Situ Scanning Tunneling Microscopic Investigation of n-Si (111). *J. Electrochem. Soc.* **1993,** *140* (4), 1009.
16. Nowicki, M.; Wandelt, K. *Metal–Electrolyte Interfaces*, John Wiley & Sons, Ltd, 2020; pp 517–731. https://doi.org/10.1002/9783527680603.ch57.
17. Wilms, M.; Kruft, M.; Bermes, G.; Wandelt, K. A New and Sophisticated Electrochemical Scanning Tunneling Microscope Design for the Investigation of Potentiodynamic Processes. *Rev. Sci. Instrum.* **1999,** *70* (9), 3641–3650. https://doi.org/10.1063/1.1149971.
18. Nirmalraj, P. N.; Thompson, D.; Riel, H. E. Capturing the Embryonic Stages of Self-Assembly—Design Rules for Molecular Computation. *Sci. Rep.* **2015,** *5* (1), 10116. https://doi.org/10.1038/srep10116.
19. Magnussen, O. M. Atomic-Scale Insights Into Electrode Surface Dynamics by High-Speed Scanning Probe Microscopy. *Chem. Eur. J.* **2019,** *25* (56), 12865–12883. https://doi.org/10.1002/chem.201901709.
20. Bryant, A.; Smith, D. P. E.; Quate, C. F. Imaging in Real Time With the Tunneling Microscope. *Appl. Phys. Lett.* **1986,** *48* (13), 832–834. https://doi.org/10.1063/1.96682.
21. Park, S.; Quate, C. F. Tunneling Microscopy of Graphite in Air. *Appl. Phys. Lett.* **1986,** *48* (2), 112–114. https://doi.org/10.1063/1.96968.
22. Robinson, R. S. Increasing the Scanning Speed of Scanning Tunnelling Microscopes. *J. Microsc.* **1988,** *152* (2), 387–397. https://onlinelibrary.wiley.com/doi/pdf/10.1111/j.1365-2818.1988.tb01400.x.
23. Ludwig, C.; Gompf, B.; Glatz, W.; Petersen, J.; Eisenmenger, W.; Möbus, M.; Zimmermann, U.; Karl, N. Video-STM, LEED and X-ray Diffraction Investigations of PTCDA on Graphite. *Zeitschrift für Physik B Condensed Matter* **1992,** *86* (3), 397–404. https://doi.org/10.1007/BF01323733.
24. Mamin, H. J.; Birk, H.; Wimmer, P.; Rugar, D. High-Speed Scanning Tunneling Microscopy: Principles and Applications. *J. Appl. Phys.* **1993,** *75* (1), 161–168. https://doi.org/10.1063/1.355877.
25. Wintterlin, J.; Trost, J.; Renisch, S.; Schuster, R.; Zambelli, T.; Ertl, G. Real-Time STM Observations of Atomic Equilibrium Fluctuations in an Adsorbate System: O/Ru(0001). *Surf. Sci.* **1997,** *394* (1), 159–169. http://www.sciencedirect.com/science/article/pii/S0039602897006043.
26. Magnussen, O. M.; Polewska, W.; Zitzler, L.; Behm, R. J. In Situ Video-STM Studies of Dynamic Processes at Electrochemical Interfaces. *Faraday Discuss.* **2002,** *121,* 43–52.
27. Yanson, Y. I.; Schenkel, F.; Rost, M. J. Design of a High-Speed Electrochemical Scanning Tunneling Microscope. *Rev. Sci. Instrum.* **2013,** *84* (2), 023702. https://doi.org/10.1063/1.4779086.
28. Yoshioka, T.; Matsushima, H.; Ueda, M. In Situ Observation of Cu Electrodeposition and Dissolution on Au(100) by High-Speed Atomic Force Microscopy. *Electrochem. Commun.* **2018,** *92,* 29–32. https://doi.org/10.1016/j.elecom.2018.05.019.
29. Ando, T. High-Speed AFM Imaging. *Curr. Opin. Struct. Biol.* **2014,** *28,* 63–68. https://doi.org/10.1016/j.sbi.2014.07.011.
30. Fukui, T.; Uchihashi, T.; Sasaki, N.; Watanabe, H.; Takeuchi, M.; Sugiyasu, K. Direct Observation and Manipulation of Supramolecular Polymerization by High-Speed Atomic Force Microscopy. *Angew. Chem. Int. Ed.* **2018,** *57* (47), 15465–15470. https://onlinelibrary.wiley.com/doi/pdf/10.1002/anie.201809165.
31. Esch, F.; Dri, C.; Spessot, A.; Africh, C.; Cautero, G.; Giuressi, D.; Sergo, R.; Tommasini, R.; Comelli, G. The Fast Module: An Add-on Unit for Driving Commercial Scanning Probe Microscopes at Video Rate and Beyond. *Rev. Sci. Instrum.* **2011,** *82* (5), 053702. https://doi.org/10.1063/1.3585984.
32. Dri, C.; Panighel, M.; Tiemann, D.; Patera, L. L.; Troiano, G.; Fukamori, Y.; Knoller, F.; Lechner, B. A. J.; Cautero, G.; Giuressi, D.; Comelli, G.; Fraxedas, J.; Africh, C.; Esch, F. The New FAST Module: A Portable and Transparent Add-on Module for Time-Resolved Investigations With Commercial Scanning Probe Microscopes. *Ultramicroscopy* **2019,** *205,* 49–56. https://www.sciencedirect.com/science/article/pii/S0304399118304169.
33. Besenbacher, F.; Lægsgaard, E.; Stensgaard, I. Fast-Scanning STM Studies. *Mater. Today* **2005,** *8* (5), 26–30. https://doi.org/10.1016/S1369-7021(05)00843-6.
34. Kuipers, L.; Loos, R. W. M.; Neerings, H.; ter Horst, J.; Ruwiel, G. J.; de Jongh, A. P.; Frenken, J. W. M. Design and Performance of a High-Temperature, High-Speed Scanning Tunneling Microscope. *Rev. Sci. Instrum.* **1995,** *66* (9), 4557–4565. https://doi.org/10.1063/1.1145289.
35. Curtis, R.; Mitsui, T.; Ganz, E. An Ultrahigh Vacuum High Speed Scanning Tunneling Microscope. *Rev. Sci. Instrum.* **1997,** *68* (7), 2790–2796. https://doi.org/10.1063/1.1148196.
36. Nakakura, C. Y.; Phanse, V. M.; Zheng, G.; Bannon, G.; Altman, E. I.; Lee, K. P. A High-Speed Variable-Temperature Ultrahigh Vacuum Scanning Tunneling Microscope. *Rev. Sci. Instrum.* **1998,** *69* (9), 3251–3258. https://doi.org/10.1063/1.1149224.
37. Pan, S. H.; Hudson, E. W.; Davis, J. C. 3He Refrigerator Based Very Low Temperature Scanning Tunneling Microscope. *Rev. Sci. Instrum.* **1999,** *70* (2), 1459–1463. https://doi.org/10.1063/1.1149605.
38. Petersen, L.; Schunack, M.; Schaefer, B.; Linderoth, T. R.; Rasmussen, P. B.; Sprunger, P. T.; Laegsgaard, E.; Stensgaard, I.; Besenbacher, F. A Fast-Scanning, Low- and Variable-Temperature Scanning Tunneling Microscope. *Rev. Sci. Instrum.* **2001,** *72* (2), 1438–1444. https://doi.org/10.1063/1.1337068.
39. Rost, M. J.; Crama, L.; Schakel, P.; van Tol, E.; van Velzen-Williams, G. B. E. M.; Overgauw, C. F.; ter Horst, H.; Dekker, H.; Okhuijsen, B.; Seynen, M.; Vijftigschild, A.; Han, P.; Katan, A. J.; Schoots, K.; Schumm, R.; van Loo, W.; Oosterkamp, T. H.; Frenken, J. W. M. Scanning Probe Microscopes Go Video Rate and Beyond. *Rev. Sci. Instrum.* **2005,** *76* (5), 053710. https://doi.org/10.1063/1.1915288.
40. Schitter, G.; Rost, M. J. Scanning Probe Microscopy at Video-Rate. *Mater. Today* **2008,** *11,* 40–48. https://www.sciencedirect.com/science/article/pii/S1369702109700069.
41. Rost, M. J.; van Baarle, G. J. C.; Katan, A. J.; van Spengen, W. M.; Schakel, P.; van Loo, W. A.; Oosterkamp, T. H.; Frenken, J. W. M. Video-Rate Scanning Probe Control Challenges: Setting the Stage for a Microscopy Revolution. *Asian J. Control* **2009,** *11* (2), 110–129. https://doi.org/10.1002/asjc.88.
42. Yang, Y.-C.; Magnussen, O. M. Thiolate-Induced Surface Reconstruction of Cu(100) Electrodes Studied by In Situ Video-STM. *J. Electroanal. Chem.* **2014,** *716* (Suppl. C), 80–86. Special Issue in Honour of Kingo Itaya. http://www.sciencedirect.com/science/article/pii/S1572665713004396.
43. Frenken, J.; Groot, I. Seeing Dynamic Phenomena With Live Scanning Tunneling Microscopy. *MRS Bull.* **2017,** *42* (11), 834–841. https://doi.org/10.1557/mrs.2017.239.
44. Yang, Z.; Gura, L.; Kalaß, F.; Marschalik, P.; Brinker, M.; Kirstaedter, W.; Hartmann, J.; Thielsch, G.; Junkes, H.; Heyde, M.; Freund, H.-J. A High-Speed Variable-Temperature Ultrahigh Vacuum Scanning Tunneling Microscope With Spiral Scan Capabilities. *Rev. Sci. Instrum.* **2022,** *93* (5), 053704. https://doi.org/10.1063/5.0079868.
45. Croft, D.; Devasia, S. Vibration Compensation for High Speed Scanning Tunneling Microscopy. *Rev. Sci. Instrum.* **1999,** *70* (12), 4600–4605. https://doi.org/10.1063/1.1150119.
46. Nanonis, Nanonis SPM Control System. https://www.specs-group.com/nanonis/products/mimea/.
47. Leiden, Leiden Preamplifier. https://leidenprobemicroscopy.com/support-equipment/.
48. Vmebus, Sis3316 Digitizer. https://www.struck.de/sis3316.html.

49. Falco-Systems, High Speed High Voltage Amplifier WMA-300. https://www.falco-systems.com/products.html.
50. Hosaka, S.; Hasegawa, T.; Hosoki, S.; Takata, K. Fast Scanning Tunneling Microscope for Dynamic Observation. *Rev. Sci. Instrum.* **1990,** *61* (4), 1342–1343. https://doi.org/10.1063/1.1141189.
51. Rost, M. High-Speed Electrochemical STM. In *Encyclopedia of Interfacial Chemistry;* Wandelt, K., Ed., Elsevier: Oxford, 2018; pp 180–198. https://doi.org/10.1016/B978-0-12-409547-2.13622-4.
52. Bastiaans, K. M.; Benschop, T.; Chatzopoulos, D.; Cho, D.; Dong, Q.; Jin, Y.; Allan, M. P. Amplifier for Scanning Tunneling Microscopy at MHz Frequencies. *Rev. Sci. Instrum.* **2018,** *89* (9), 093709. https://doi.org/10.1063/1.5043267.
53. Xu, C.; Que, Y.; Zhuang, Y.; Wang, K.; Xiao, X. Construction of a Gigahertz-Bandwidth Radio-Frequency Scanning Tunneling Microscope Based on a Commercial Low-Temperature System. *Rev. Sci. Instrum.* **2019,** *90* (10), 103706. https://doi.org/10.1063/1.5109721.
54. Li, Q. F.; Wang, Y.; Wang, F.; Hou, Y.; Lu, Q. 100 MHz Large Bandwidth Preamplifier and Record-Breaking 50 kHz Scanning Rate Quantum Point Contact Mode Probe Microscopy Imaging With Atomic Resolution. *Rev. Sci. Instrum.* **2021,** *92* (1), 013701. https://doi.org/10.1063/5.0024802.
55. Junkes, H.; Freund, H.-J.; Gura, L.; Heyde, M.; Marschalik, P.; Yang, Z. Experiment Control With EPICS7 and Symmetric Multiprocessing on RTEMS. In *16th International Conference on Accelerator and Large Experimental Control Systems (ICALEPCS2017)*, JACoW, 2018; pp 1762–1766.
56. Gura, L.; Yang, Z.; Brinker, M.; Kalaß, F.; Kirstaedter, W.; Marschalik, P.; Junkes, H.; Heyde, M.; Freund, H.-J. Spiral High-Speed Scanning Tunneling Microscopy: Tracking Atomic Diffusion on the Millisecond Timescale. *Appl. Phys. Lett.* **2021,** *119* (25), 251601. https://doi.org/10.1063/5.0071340.
57. Leonard Gura, M. B. Point Cloud Visualization and Analysis. *GitHub Repository* **2021**. https://github.molgen.mpg.de/gura/point_cloud_visualization_and_analyis.
58. Andersson, S. B.; Abramovitch, D. Y. A Survey of Non-raster Scan Methods With Application to Atomic Force Microscopy. In *2007 American Control Conference;* 2007; pp 3516–3521.
59. Wang, J.; Wang, J.; Hou, Y.; Lu, Q. Self-Manifestation and Universal Correction of Image Distortion in Scanning Tunneling Microscopy With Spiral Scan. *Rev. Sci. Instrum.* **2010,** *81* (7), 073705. https://doi.org/10.1063/1.3449322.
60. Hung, S.-K. Spiral Scanning Method for Atomic Force Microscopy. *J. Nanosci. Nanotechnol.* **2010,** *10* (7), 4511–4516.
61. Bazaei, A.; Yong, Y. K.; Moheimani, S. O. R. High-Speed Lissajous-Scan Atomic Force Microscopy: Scan Pattern Planning and Control Design Issues. *Rev. Sci. Instrum.* **2012,** *83* (6), 063701. https://doi.org/10.1063/1.4725525.
62. Tuma, T.; Lygeros, J.; Kartik, V.; Sebastian, A.; Pantazi, A. High-Speed Multiresolution Scanning Probe Microscopy Based on Lissajous Scan Trajectories. *Nanotechnology* **2012,** *23* (18), 185501. https://doi.org/10.1088/0957-4484/23/18/185501.
63. Ziegler, D.; Meyer, T. R.; Farnham, R.; Brune, C.; Bertozzi, A. L.; Ashby, P. D. Improved Accuracy and Speed in Scanning Probe Microscopy by Image Reconstruction From Non-gridded Position Sensor Data. *Nanotechnology* **2013,** *24* (33), 335703. https://doi.org/10.1088/0957-4484/24/33/335703.
64. Rana, M. S.; Pota, H. R.; Petersen, I. R. Spiral Scanning With Improved Control for Faster Imaging of AFM. *IEEE Trans. Nanotechnol.* **2014,** *13* (3), 541–550. https://doi.org/10.1109/TNANO.2014.2309653.
65. Ziegler, D.; Meyer, T. R.; Amrein, A.; Bertozzi, A. L.; Ashby, P. D. Ideal Scan Path for High-Speed Atomic Force Microscopy. *IEEE/ASME Trans. Mechatron.* **2017,** *22* (1), 381–391.
66. Teo, Y. R.; Yong, Y.; Fleming, A. J. A Comparison of Scanning Methods and the Vertical Control Implications for Scanning Probe Microscopy. *Asian J. Control* **2018,** *20* (4), 1352–1366. https://onlinelibrary.wiley.com/doi/pdf/10.1002/asjc.1422.
67. Das, S. K.; Badal, F. R.; Rahman, M. A.; Islam, M. A.; Sarker, S. K.; Paul, N. Improvement of Alternative Non-raster Scanning Methods for High Speed Atomic Force Microscopy: A Review. *IEEE Access* **2019,** *7,* 115603–115624.
68. Sun, Z.; Xi, N.; Xue, Y.; Cheng, Y.; Chen, L.; Yang, R.; Song, B. Task Space Motion Control for AFM-Based Nanorobot Using Optimal and Ultralimit Archimedean Spiral Local Scan. *IEEE Robot. Autom. Lett.* **2019,** *5* (2), 282–289.
69. Yong, Y. K.; Moheimani, S. O. R.; Petersen, I. R. High-Speed Cycloid-Scan Atomic Force Microscopy. *Nanotechnology* **2010,** *21* (36), 365503. http://stacks.iop.org/0957-4484/21/i=36/a=365503.
70. Mahmood, I. A.; Moheimani, S. R.; Bhikkaji, B. A New Scanning Method for Fast Atomic Force Microscopy. *IEEE Trans. Nanotechnol.* **2011,** *10* (2), 203–216.
71. Yong, Y. K.; Bazaei, A.; Moheimani, S. O. R.; Allgöwer, F. Design and Control of a Novel Non-raster Scan Pattern for Fast Scanning Probe Microscopy. In *IEEE/ASME International Conference on Advanced Intelligent Mechatronics*, AIM, 2012; pp 456–461.
72. Yong, Y. K.; Bazaei, A.; Moheimani, S. R. Video-Rate Lissajous-Scan Atomic Force Microscopy. *IEEE Trans. Nanotechnol.* **2014,** *13* (1), 85–93.
73. Gura, L.; Yang, Z.; Paier, J.; Kalaß, F.; Brinker, M.; Junkes, H.; Heyde, M.; Freund, H.-J. Resolving Atomic Diffusion in Ru(0001)-O(2×2) With Spiral High-Speed Scanning Tunneling Microscopy. *Phys. Rev. B* **2022,** *105,* 035411. https://doi.org/10.1103/PhysRevB.105.035411.
74. Gura, L.; Yang, Z.; Paier, J.; Kalaß, F.; Brinker, M.; Junkes, H.; Heyde, M.; Freund, H.-J. Dynamics in the O(2×1) Adlayer on Ru(0001): Bridging Timescales From Milliseconds to Minutes by Scanning Tunneling Microscopy. *Phys. Chem. Chem. Phys.* **2022,** *24,* 15265–15270. https://doi.org/10.1039/D2CP02363F.
75. Li, Q.; Lu, Q. Atomic Resolution Ultrafast Scanning Tunneling Microscope With Scan Rate Breaking the Resonant Frequency of a Quartz Tuning Fork Resonator. *Rev. Sci. Instrum.* **2011,** *82* (5), 053705. https://doi.org/10.1063/1.3585200.
76. Henß, A.-K.; Wiechers, J.; Schuster, R.; Platschkowski, V.; Wintterlin, J. A Beetle-Type, Variable-Temperature Scanning Tunneling Microscope for Video-Rate Imaging. *Jpn. J. Appl. Phys.* **2020,** *59* (SN), SN1007. https://doi.org/10.35848/1347-4065/ab8680.
77. Henß, A.-K.; Sakong, S.; Messer, P. K.; Wiechers, J.; Schuster, R.; Lamb, D. C.; Groß, A.; Wintterlin, J. Density Fluctuations as Door-Opener for Diffusion on Crowded Surfaces. *Science* **2019,** *363* (6428), 715. http://science.sciencemag.org/content/363/6428/715.abstract.
78. Patera, L. L.; Bianchini, F.; Africh, C.; Dri, C.; Soldano, G.; Mariscal, M. M.; Peressi, M.; Comelli, G. Real-Time Imaging of Adatom-Promoted Graphene Growth on Nickel. *Science* **2018,** *359* (6381), 1243–1246. https://www.science.org/doi/pdf/10.1126/science.aan8782.
79. Yang, Y.-C.; Taranovskyy, A.; Magnussen, O. M. In Situ Video-STM Studies of Methyl Thiolate Surface Dynamics and Self-Assembly on Cu(100) Electrodes. *Langmuir* **2012,** *28* (40), 14143–14154. https://doi.org/10.1021/la302939f.
80. Sang, X.; Lupini, A. R.; Unocic, R. R.; Chi, M.; Borisevich, A. Y.; Kalinin, S. V.; Endeve, E.; Archibald, R. K.; Jesse, S. Dynamic Scan Control in STEM: Spiral Scans. *Adv. Struct. Chem. Imaging* **2016,** *2* (1), 6.
81. Momotenko, D.; Byers, J. C.; McKelvey, K.; Kang, M.; Unwin, P. R. High-Speed Electrochemical Imaging. *ACS Nano* **2015,** *9* (9), 8942–8952. https://doi.org/10.1021/acsnano.5b02792.
82. Wang, Q.; Hou, Y.; Wang, J.; Lu, Q. A High-Stability Scanning Tunneling Microscope Achieved by an Isolated Tiny Scanner With Low Voltage Imaging Capability. *Rev. Sci. Instrum.* **2013,** *84* (11), 113703. https://doi.org/10.1063/1.4829716.
83. Sapountzi, F. M.; Gracia, J. M.; Weststrate, C. J. K.-J.; Fredriksson, H. O. A.; Niemantsverdriet, J. W. H. Electrocatalysts for the Generation of Hydrogen, Oxygen and Synthesis Gas. *Prog. Energy Combust. Sci.* **2017,** *58,* 1–35. https://www.sciencedirect.com/science/article/pii/S0360128516300260.
84. Emmez, E.; Anibal Boscoboinik, J.; Tenney, S.; Sutter, P.; Shaikhutdinov, S.; Freund, H.-J. Oxidation of the Ru(0001) Surface Covered by Weakly Bound, Ultrathin Silicate Films. *Surf. Sci.* **2016,** *646,* 19–25. Heterogeneous Catalysis, a Special Issue Honour Richard Lambert. https://www.sciencedirect.com/science/article/pii/S0039602815001776.
85. Włodarczyk, R.; Sierka, M.; Sauer, J.; Löffler, D.; Uhlrich, J. J.; Yu, X.; Yang, B.; Groot, I. M. N.; Shaikhutdinov, S.; Freund, H.-J. Tuning the Electronic Structure of Ultrathin Crystalline Silica Films on Ru(0001). *Phys. Rev. B* **2012,** *85* (8), 085403. https://link.aps.org/doi/10.1103/PhysRevB.85.085403.
86. Li, T.; Yarmoff, J. A. Intercalation and Desorption of Oxygen Between Graphene And Ru(0001) Studied With Helium Ion Scattering. *Phys. Rev. B* **2017,** *96* (15), 155441. https://link.aps.org/doi/10.1103/PhysRevB.96.155441.
87. Voloshina, E.; Berdunov, N.; Dedkov, Y. Restoring a Nearly Free-Standing Character of Graphene on Ru(0001) by Oxygen Intercalation. *Sci. Rep.* **2016,** *6* (1), 20285. https://doi.org/10.1038/srep20285.

88. Souda, R.; Aizawa, T. Nucleation and Growth of Water Ice on Ru(0001): Influences of Oxygen and Carbon-Monoxide Adspecies. *Chem. Phys. Lett.* **2019,** *722,* 132–139. https://www.sciencedirect.com/science/article/pii/S0009261419301782.
89. Jacoby, M. Hunting for the Hidden Chemistry in Solid Catalysts. *Chem. Eng. News* **2017,** *95* (29), 28–32.